

# Rank Minimization Method for Speckle Noise Removal in Ultrasound Images

Hui-Yin Yan, Yu-Peng Liu, He-Xian Wang, and Hao Chen

**Abstract**—Ultrasound image plays an important role in many medical applications. However, images acquired in ultrasound imaging system are always corrupted by a kind of speckle noise, which seriously affects the images' qualities. In this paper, by exploiting image nonlocal similarities, we establish a maximum a posteriori (MAP) estimation-based matrix rank minimization model for speckle noise reduction, and design an alternating proximal gradient algorithm to solve the nonconvex optimization model. The convergence of the alternating proximal gradient algorithm is analyzed and proved. A image denoising method is finally developed by using the rank minimization model and its solving algorithm. Numerical experiments illustrate that the proposed denoising method can outperform some state-of-the-art methods for speckle noise removal in images.

**Index Terms**—ultrasound image denoising, speckle noise, low-rank minimization, proximal gradient algorithm.

## I. INTRODUCTION

IMAGE denoising has long-time been a fundamental problem in image processing and computer vision [1], [2]. In the literatures, efficient denoising methods are always developed for the additive white Gaussian noise removal [3]–[8]. In many practical applications, however, images are often corrupted by different kinds of non-Gaussian noises, such as Poisson noise, impulse noise and multiplicative speckle noise, etc [9]–[15]. For instance, ultrasound image plays an important role in the applications of clinical examination and diagnose [16]–[18]. Due to the coherent nature of ultrasound imaging system, the obtained images are often contaminated by a speckle noise, in which the noise reduces the image's qualities by a point-wise multiplication of image pixels. In mathematics, the degraded ultrasound image is represented by

$$g = f + \sqrt{f}v, \quad (1)$$

where  $g$  is the observed noisy image,  $f$  is the ideal clean image and  $v$  is the zero mean white Gaussian noise, respectively.

Since almost all of pixels in  $f$  may be contaminated, the restoration of  $f$  from  $g$  is a very challenging image denoising problem. In the past decades, various of methods have been

studied to suppress this kind of noise. For instance, the earliest class of methods are the filter methods, such as the local statistical properties-based filter methods [19], adaptive filter methods [20], weighted median filter methods [21], and wavelet-based filter methods [22]–[24]. Nevertheless, these methods lack the abilities to reconstruct high quality images and often result lower spatial resolution images with over smoothed edges and textures. The other class of popular methods for ultrasound image denoising is the total variation (TV)-based methods. The TV method was firstly proposed for the additive white Gaussian noise removal problem [3]. Since it has the advantages to reduce image noise and preserve image details well. In [25], Rudin et al. extended the TV method to speckle noise removal and designed efficient image restoration methods for images contaminated by Gaussian multiplicative noise. Later, the Gamma distribution multiplicative speckle noise removal problem was further studied, and Aubert and Aujol [26] developed a nonconvex TV model via the maximum a posteriori (MAP) estimation. Jin and Yang [27] similarly established a MAP-based nonconvex TV model for ultrasound image denoising. Huang and Yang further improved the nonconvex model [27] and developed a convex TV model by replacing the MAP data-fitting term with a generalized Kullback-Leibler distance [28]. Besides, to improve the classical TV-based methods, the high-order total variation (HTV) [29], total generalized variation (TGV) [30], [31], and some hybrid regularization methods have been also proposed for ultrasound image denoising. For example, in [32], Mei et al. developed a second-order TGV method to suppress speckle noise in ultrasound images. In [33], Wang et al. investigated a HTV-based variational model for speckle noise reduction. In [34], Abraham and Kadah proposed a hybrid framework combing wavelet shrinkage and total variation for clinical ultrasound image denoising.

The above mentioned methods are all local prior-based methods, which suppress image noise only using local information in image. In recent years, there are nonlocal structural sparsity and low-rank priors that have been widely exploited for image denoising and restoration [4]–[7], [35]–[37]. For instance, the block matching and 3D filtering (BM3D) method [7], which uses the stack of nonlocal similar image patches to form collaborative filters, has been extended to ultrasound image denoising and obtained significant image denoising improvements [38]. Moreover, based on image nonlocal similarities [4], [5], image nonlocal low-rank prior has been also exploited for ultrasound image denoising. The nonlocal low-rank prior on images is exploited by stacking similar patches into a stacked patch matching matrix. Due to the similarity of image patches, the patch matching matrix should be low-rank [35] and thus many image denoising and restoration problems are converted into the matrix low-rank minimization (LRM) problems [39]–[42]. Owing to

Manuscript received January 25, 2025; revised April 15, 2025. This work was supported in part by Nanhu Scholar Program for Young Scholars of XYNNU.

Hui-Yin Yan is a lecturer at the School of Mathematics and Statistics, Xinyang Normal University, Xinyang, 464000, P. R. China (Corresponding author, E-mail: yanhuiyin@xynu.edu.cn).

Yu-Peng Liu is a postgraduate at the School of Mathematics and Statistics, Xinyang Normal University, Xinyang, 464000, P. R. China (E-mail: 11527404093@163.com).

He-Xian Wang is an undergraduate at the International Education College, Xinyang Normal University, Xinyang, 464000, P. R. China (E-mail: 15516466658@163.com).

Hao Chen is a lecturer at the School of Information Engineering, Nanyang Vocational College of Agriculture, Nanyang, 473000, P. R. China (E-mail: 534361090@qq.com).

the direct matrix rank minimization is NP-hard problem, it always uses nuclear norm minimization to relax the problem. Because nuclear norm is defined to be the sum of a matrix's all singular values and proved to be the convex envelope of matrix rank function [39]. Later, by introducing different weights in nuclear norm, the more accurate approximation weighted nuclear norm minimization (WNNM) was further proposed and applied to image denoising and many low-level vision tasks [40]–[42]. Some recent LRM methods for speckle noise reduction can be referenced as follows. In [43], Liu et al. investigated multiplicative speckle noise removal and developed a nonconvex logdet-based nonlocal LRM model. In [44], Lv et al. proposed a patchwise WNNM method based on MAP estimation for speckle noise removal, and developed its alternating direction method with multipliers (ADMM). In [45], Bo et al. studied the WNNM-based model and algorithm for SAR image denoising. In [46], Yang et al. developed a WNNM framework combined with a data derived model for restoration of ultrasound images.

In this paper, we utilize the direct matrix rank minimization to develop a LRM-based method for speckle noise removal. Based on image nonlocal similarities, we firstly propose a matrix rank minimization (RM) model for patch matching matrix denoising. The RM model consists of a RM regularization term and a MAP estimation-based data fidelity term, which is in fact a nonconvex and nonsmooth optimization problem. We then design an alternating proximal gradient (APG) method to solve the nonconvex RM model and further analyze the convergence for the APG method. By adopting the RM model and its APG method to denoise all patch matching matrices formed in the noisy image and rearrange these denoised patches into image, we finally obtain the RM-based ultrasound image denoising method. Numerical experiments show that the proposed method can overcome some current state-of-the-art methods for reducing speckle noise in images.

The paper is organized as follows. In Section II, the RM speckle noise reduction model is introduced. In Section III, the APG solving algorithm is developed for the RM model. In Section IV, convergence theorems of the APG algorithm are presented. Numerical experiments are given in Section V to show the denoising effects of the proposed RM-based speckle noise reduction method. Some conclusions are finally made in Section VI.

## II. PROPOSED RANK MINIMIZATION MODEL

Suppose  $g^r$  is a  $s$ -by- $s$  reference patch in noisy image  $g$ . Based on image nonlocal similarities, there must exist  $t$  most similar patches to  $g^r$  in the image. By aggregating these similar patches to be a  $s^2$ -by- $t$  patch matching matrix  $X$ , the image degradation model (1) implies that

$$Y = X + \sqrt{X}V, \quad (2)$$

where  $X$  and  $V$  are the  $s^2$ -by- $t$  patch matching matrix formed in clean image  $f$ , and corresponding noise matrix, respectively. In [44], Lv et al. established a patch-based WNNM model to denoise  $V$  in (2), which is

$$\min_X \sum_{i,j} \frac{(X_{i,j} - Y_{i,j})^2}{X_{i,j}} + \|X\|_{w,*}, \quad (3)$$

where  $\sum_{i,j} \frac{(X_{i,j} - Y_{i,j})^2}{X_{i,j}}$  is the MAP estimation-based data fidelity term.  $\|X\|_{w,*} = \sum \omega_l \sigma_l$  is the weighted nuclear norm regularization term, with  $\sigma_l$  and  $\omega_l$  to be the  $l$ -th singular value of  $X$  and which corresponding weight parameter.

In this paper, we improve the LRM model (3) by replacing the weighted nuclear norm with matrix rank,

$$\min_X \sum_{i,j} \frac{(X_{i,j} - Y_{i,j})^2}{X_{i,j}} + \omega \text{Rank}(X), \quad (4)$$

where  $\text{Rank}(\cdot)$  represents the matrix's rank and  $\omega$  is a regularization parameter. By introducing an auxiliary variable  $Z$  to  $X$ , (4) can be converted into the unconstraint optimization problem

$$\min_{X,Z} \mathcal{Q}(X, Z), \quad (5)$$

and

$$\mathcal{Q}(X, Z) = \sum_{i,j} \frac{(Z_{i,j} - Y_{i,j})^2}{Z_{i,j}} + \frac{\theta}{2} \|X - Z\|_F^2 + \omega \text{Rank}(X),$$

where  $\theta$  is a positive penalty parameter. As  $\theta \rightarrow \infty$ ,  $Z \rightarrow X$  and the solution of (5) tends to that of (4). Thus, the solution of (4) can be obtained by solving problem (5).

## III. ALTERNATING PROXIMAL GRADIENT METHOD

In this section, we design a novel alternating proximal gradient method to solve the nonconvex problem (5). Denoted by  $\Phi(X) = \omega \text{Rank}(X)$ ,  $\Psi(Z) = \sum_{i,j} \frac{(Z_{i,j} - Y_{i,j})^2}{Z_{i,j}}$ ,  $\mathcal{H}(X, Z) = \frac{\theta}{2} \|X - Z\|_F^2$ , the objective function  $\mathcal{Q}(X, Z)$  in (5) can be represented as

$$\mathcal{Q}(X, Z) = \Phi(X) + \mathcal{H}(X, Z) + \Psi(Z).$$

Since  $\mathcal{H}(X, Z)$  has second order differentiable with respect to variables  $X$  and  $Z$ . We can design an alternating proximal gradient scheme to solve (5).

For some initial gauss  $(X^{(0)}, Z^{(0)})$ , the  $k$ -th iteration of the scheme is to obtain

$$\begin{cases} X^{(k)} \in \arg \min_X \left\langle \nabla_X \mathcal{H}(X^{(k-1)}, Z^{(k-1)}), X - X^{(k-1)} \right\rangle \\ \quad + \frac{\alpha}{2} \|X - X^{(k-1)}\|_F^2 + \Phi(X), \\ Z^{(k)} \in \arg \min_Z \left\langle \nabla_Z \mathcal{H}(X^{(k)}, Z^{(k-1)}), Z - Z^{(k-1)} \right\rangle \\ \quad + \frac{\beta}{2} \|Z - Z^{(k-1)}\|_F^2 + \Psi(Z), \end{cases} \quad (6)$$

where  $\alpha, \beta > 0$  are larger than the Lipschitz constant of  $\mathcal{H}$ ,  $\langle \cdot \rangle$  and  $\nabla$  denotes the inter product of vectors and gradient operator of the function.

In fact, (6) can be transformed into

$$\begin{cases} X^{(k)} \in \arg \min_X \Phi(X) + \\ \quad \frac{\alpha}{2} \left\| X - X^{(k-1)} + \frac{1}{\alpha} \nabla_X \mathcal{H}(X^{(k-1)}, Z^{(k-1)}) \right\|_F^2, \\ Z^{(k)} \in \arg \min_Z \Psi(Z) + \\ \quad \frac{\beta}{2} \left\| Z - Z^{(k-1)} + \frac{1}{\beta} \nabla_Z \mathcal{H}(X^{(k)}, Z^{(k-1)}) \right\|_F^2, \end{cases} \quad (7)$$

and

$$\begin{cases} X^{(k)} \in \arg \min_X \frac{\alpha}{2} \left\| X - \left( \frac{\theta}{\alpha} Z^{(k-1)} + \frac{\tilde{\alpha}}{\alpha} X^{(k-1)} \right) \right\|_F^2 \\ \quad + \omega \text{Rank}(X), \\ Z^{(k)} \in \arg \min_Z \frac{\beta}{2} \left\| Z - \left( \frac{\theta}{\beta} X^{(k)} + \frac{\tilde{\beta}}{\beta} Z^{(k-1)} \right) \right\|_F^2 \\ \quad + \sum_{i,j} \frac{(Z_{i,j} - Y_{i,j})^2}{Z_{i,j}}, \end{cases} \quad (8)$$

where  $\tilde{\alpha} = \alpha - \theta$  and  $\tilde{\beta} = \beta - \theta$ .

For solution of  $X^{(k)}$  in (8), suppose the singular value decomposition (SVD) of  $\left( \frac{\theta}{\alpha} Z^{(k-1)} + \frac{\tilde{\alpha}}{\alpha} X^{(k-1)} \right)$  to be  $U^{(k)} \Sigma^{(k)} (V^{(k)})^T$ , the SVD-based hard threshold algorithm in [47] implies that,

$$X^{(k)} = U^{(k)} \mathcal{D}_{\frac{\omega}{\alpha}} \left( \Sigma^{(k)} \right) \left( V^{(k)} \right)^T.$$

Where  $\mathcal{D}_{\frac{\omega}{\alpha}} \left( \Sigma^{(k)} \right)$  is the hard threshold algorithm defined on diagonal matrix  $\Sigma^{(k)} = \text{diag}(\sigma_1, \sigma_2, \dots)$ , and each of its diagonal element is given by

$$\mathcal{D}_{\frac{\omega}{\alpha}} \left( \Sigma^{(k)} \right)_{ll} = \begin{cases} \sigma_l, & \text{for } \sigma_l \geq \sqrt{\frac{2\omega}{\alpha}}, \\ 0, & \text{for } \sigma_l < \sqrt{\frac{2\omega}{\alpha}}. \end{cases}$$

Since the function  $\Psi(Z)$  in (8) has second order differential about  $Z$  and every element of  $Z$  is independent to each other. Therefore,  $Z^{(k)}$  can be solved element-by-element via the Newton iteration method from

$$\min_{Z_{i,j}} \frac{(Z_{i,j} - Y_{i,j})^2}{Z_{i,j}} + \frac{\beta}{2} \left( Z_{i,j} - \frac{\tilde{\beta}}{\beta} X_{i,j}^{(k)} - \frac{\theta}{\beta} Z_{i,j}^{(k-1)} \right)^2.$$

The entire alternating proximal gradient method can be concluded in Algorithm 1.

**Algorithm 1** : Alternating proximal gradient algorithm for solving (5).

1. Initialize  $X^{(0)}$ ,  $Z^{(0)}$ , and parameters  $\theta$ ,  $\omega$ ,  $\alpha$ ,  $\beta$ .
2. **For**  $k = 1, 2, \dots$ , **do**

1) update  $X^{(k)}$  from

$$\min_X \frac{\alpha}{2} \left\| X - \frac{\theta}{\alpha} Z^{(k-1)} - \frac{\tilde{\alpha}}{\alpha} X^{(k-1)} \right\|_F^2 + \omega \text{Rank}(X);$$

2) update  $Z^{(k)}$  from

$$\min_{Z_{i,j}} \frac{\beta}{2} \left( Z_{i,j} - \frac{\theta}{\beta} X_{i,j}^{(k)} - \frac{\tilde{\beta}}{\beta} Z_{i,j}^{(k-1)} \right)^2 + \frac{(Z_{i,j} - Y_{i,j})^2}{Z_{i,j}},$$

$$1 \leq i \leq s^2, 1 \leq j \leq t;$$

**end for** until the stopping criterion is satisfied.

#### IV. CONVERGENCE ANALYSIS

In this section, the convergence theorems of the proposed alternating proximal gradient Algorithm 1 are presented. We simply denote  $\partial \mathcal{F}(x)$  as the subdifferential [48] of function  $\mathcal{F}$  at a point  $x$ , and call the point which subdifferential contains  $\mathbf{0}$  as critical point, where  $\mathbf{0}$  is the zero point. Suppose



(a)

(b)



(c)

(d)



(e)

(f)



(g)

(h)



(i)

(j)

Fig. 1. Original clean simulation images. The left column: (a) Monarch, (c) Barbara, (e) Villa, (g) Plane, (i) Baby; and the right column: (b) Boat, (d) Parrot, (f) Cameraman, (h) House, (j) Peppers; respectively.

crit $\mathcal{F}$  is the set of critical points of  $\mathcal{F}$ ,  $\|\cdot\|$  is the Euclidean norm, the convergence theorems are given as follows.

*Theorem 1:* Suppose  $\{W^{(k)}\}$  to be a sequence obtained by the alternating proximal gradient Algorithm 1,  $W^{(k)} = \left( (X^{(k)})^T, (Z^{(k)})^T \right)^T$ , then, for  $k \geq 1$ ,  $\mathcal{Q}(W^{(k)})$  does not increase,

$$\mathcal{Q}(W^{(k)}) + \frac{\tilde{\alpha}}{2} \left\| X^{(k)} - X^{(k-1)} \right\|_F^2 + \frac{\tilde{\beta}}{2} \left\| Z^{(k)} - Z^{(k-1)} \right\|_F^2 \leq \mathcal{Q}(W^{(k-1)}), \quad (9)$$

and

$$\lim_{k \rightarrow \infty} \left\| W^{(k)} - W^{(k-1)} \right\|_F^2 = 0. \quad (10)$$

*Proof:* Since it has the Taylor expansions

$$\begin{aligned} \mathcal{H}(X, Z^{(k-1)}) &= \mathcal{H}(X^{(k-1)}, Z^{(k-1)}) \\ &+ \left\langle \nabla_X \mathcal{H}(X^{(k-1)}, Z^{(k-1)}), X - X^{(k-1)} \right\rangle \\ &+ \frac{\theta}{2} \left\| X - X^{(k-1)} \right\|_F^2 \end{aligned}$$

and

$$\begin{aligned} \mathcal{H}(X^{(k)}, Z) &= \mathcal{H}(X^{(k)}, Z^{(k-1)}) \\ &+ \left\langle \nabla_Z \mathcal{H}(X^{(k)}, Z^{(k-1)}), Z - Z^{(k-1)} \right\rangle \\ &+ \frac{\theta}{2} \left\| Z - Z^{(k-1)} \right\|_F^2. \end{aligned}$$

Based on (6), we can derive that

$$X^{(k)} \in \arg \min_X \mathcal{Q}(X, Z^{(k-1)}) + \frac{\tilde{\alpha}}{2} \left\| X - X^{(k-1)} \right\|_F^2, \quad (11)$$

and

$$Z^{(k)} \in \arg \min_Z \mathcal{Q}(X^{(k)}, Z) + \frac{\tilde{\beta}}{2} \left\| Z - Z^{(k-1)} \right\|_F^2. \quad (12)$$

Therefore,

$$\begin{aligned} \mathcal{Q}(X^{(k)}, Z^{(k-1)}) + \frac{\tilde{\alpha}}{2} \left\| X^{(k)} - X^{(k-1)} \right\|_F^2 \\ \leq \mathcal{Q}(X^{(k-1)}, Z^{(k-1)}), \end{aligned}$$

and

$$\mathcal{Q}(X^{(k)}, Z^{(k)}) + \frac{\tilde{\beta}}{2} \left\| Z^{(k)} - Z^{(k-1)} \right\|_F^2 \leq \mathcal{Q}(X^{(k)}, Z^{(k-1)}).$$

Combining the above two formulas,

$$\begin{aligned} \mathcal{Q}(W^{(k)}) + \frac{\tilde{\alpha}}{2} \left\| X^{(k)} - X^{(k-1)} \right\|_F^2 \\ + \frac{\tilde{\beta}}{2} \left\| Z^{(k)} - Z^{(k-1)} \right\|_F^2 \leq \mathcal{Q}(W^{(k-1)}). \end{aligned}$$

Thus,  $\mathcal{Q}(W^{(k)})$  does not increase with the increase of  $k$ .

By summing each inequality (9) from  $k = 1$  to  $K_0$ , it satisfies that

$$\begin{aligned} \sum_{k=1}^{K_0} \left( \frac{\tilde{\alpha}}{2} \left\| X^{(k)} - X^{(k-1)} \right\|_F^2 + \frac{\tilde{\beta}}{2} \left\| Z^{(k)} - Z^{(k-1)} \right\|_F^2 \right) \\ \leq \mathcal{Q}(W^{(0)}) - \mathcal{Q}(W^{(K_0)}). \quad (13) \end{aligned}$$

Since  $\tilde{\alpha}$  and  $\tilde{\beta}$  are bounded constants, it follows by (13) that

$$\lim_{K_0 \rightarrow \infty} \sum_{k=1}^{K_0} \left\| W^{(k)} - W^{(k-1)} \right\|_F^2 < +\infty,$$

and

$$\lim_{k \rightarrow \infty} \left\| W^{(k)} - W^{(k-1)} \right\|_F^2 = 0. \quad \blacksquare$$

**Algorithm 2 :** The ultrasound image denoising method.

1. Input the noisy image  $g$ , initialize parameters  $s, t, \theta, \omega, \alpha, \beta$ , and set  $k = 1$  and the maximum iteration number  $K$ .
2. Divide  $p$  reference patches in  $g$ , and initialize the  $s^2 \times t$  initial patch matching matrices  $Y_1^{(0)}, Y_2^{(0)}, \dots, Y_p^{(0)}$  by conducting the image block matching schemes on  $g$ .
3. **When**  $k < K$ , **do**
- 1) **for**  $\zeta = 1, 2, \dots, p$ , apply alternating proximal gradient Algorithm 1 to solve  $X_\zeta^{(k)}$  from

$$\min_{X_\zeta} \sum_{i,j} \frac{\left( X_\zeta - Y_\zeta^{(k-1)} \right)_{i,j}^2}{X_{i,j}} + \omega \text{Rank}(X_\zeta),$$

**end for;**

- 2) aggregate  $X_1^{(k)}, X_2^{(k)}, \dots, X_p^{(k)}$  to form the denoised image  $\hat{f}^{(k)}$ ;
  - 3) update the patch matching matrices  $Y_1^{(k)}, Y_2^{(k)}, \dots, Y_p^{(k)}$  from  $\hat{f}^{(k)}$ ;
  - 4) if  $k > K$ , stop, else  $k := k + 1$  and go back to the step 3;
- end for** and output the finally denoised image  $\hat{f}^{(k)}$ .

*Theorem 2:* Suppose  $\{W^{(k)}\}$  to be a sequence obtained by the alternating proximal gradient Algorithm 1,  $W^{(k)} = \left( (X^{(k)})^T, (Z^{(k)})^T \right)^T$ , denote by

$$\hat{X}^{(k)} = \theta \left( Z^{(k-1)} - Z^{(k)} \right) - \alpha \left( X^{(k)} - X^{(k-1)} \right),$$

and

$$\hat{Z}^{(k)} = -\tilde{\beta} \left( Z^{(k)} - Z^{(k-1)} \right).$$

Then, for  $k \geq 1$ ,

$$\widehat{W}^{(k)} = \left( \left( \hat{X}^{(k)} \right)^T, \left( \hat{Z}^{(k)} \right)^T \right)^T \in \partial \mathcal{Q}(W^{(k)}),$$

and

$$\left\| \widehat{W}^{(k)} \right\|_F \leq c \left\| W^{(k)} - W^{(k-1)} \right\|_F, \quad (14)$$

where  $c$  is a bounded constant.

*Proof:* For all  $k \geq 1$ , the solving of  $X^{(k)}$  in (7) suggests that

$$\begin{aligned} \mathbf{0} \in \alpha \left( X^{(k)} - X^{(k-1)} \right) \\ + \theta \left( X^{(k)} - Z^{(k-1)} \right) + \omega \partial \text{Rank} \left( X^{(k)} \right), \end{aligned}$$

where  $\mathbf{0} \in \mathbb{R}^{s^2 \times t}$  and  $\partial \text{Rank}(\cdot)$  is the subdifferential of the matrix rank function. By adding  $-\theta Z^{(k)}$  at both sides of the

above equation,

$$-\theta Z^{(k)} \in \alpha \left( X^{(k)} - X^{(k-1)} \right) + \theta \left( X^{(k)} - Z^{(k-1)} - Z^{(k)} \right) + \omega \partial \text{Rank} \left( X^{(k)} \right),$$

and for  $k \geq 1$ , which implies that

$$\begin{aligned} \widehat{X}^{(k)} &= \theta \left( Z^{(k-1)} - Z^{(k)} \right) - \alpha \left( X^{(k)} - X^{(k-1)} \right) \\ &\in \theta \left( X^{(k)} - Z^{(k)} \right) + \omega \partial \text{Rank} \left( X^{(k)} \right). \end{aligned} \quad (15)$$

Analogously, for all  $k \geq 1$ , the solving of  $Z^{(k)}$  in (7) also implies that

$$\mathbf{0} = \nabla_Z \mathcal{Q} \left( X^{(k)}, Z^{(k)} \right) + \widetilde{\beta} \left( Z^{(k)} - Z^{(k-1)} \right),$$

and

$$\widehat{Z}^{(k)} = -\widetilde{\beta} \left( Z^{(k)} - Z^{(k-1)} \right) = \nabla_Z \mathcal{Q} \left( X^{(k)}, Z^{(k)} \right), \quad (16)$$

where  $\nabla_Z$  denotes the derivation of the function  $\mathcal{Q} \left( X^{(k)}, Z^{(k)} \right)$  about  $Z$ . The subdifferential calculation formulations of variable separated functions [48] imply that, for any  $W = (X^T, Z^T)^T \in \text{dom} \mathcal{Q}$ ,

$$\begin{aligned} \partial \mathcal{Q}(W) &= \partial_X \mathcal{Q}(W) \times \partial_Z \mathcal{Q}(W) \\ &= [\theta(X - Z) + \omega \partial \text{Rank}(X)] \times \nabla_Z \mathcal{Q}(W). \end{aligned}$$

Therefore, it can be derived by (15) and (16) that

$$\widehat{W}^{(k)} = \left( \left( \widehat{X}^{(k)} \right)^T, \left( \widehat{Z}^{(k)} \right)^T \right)^T \in \partial \mathcal{Q} \left( W^{(k)} \right),$$

and

$$\begin{aligned} \left\| \widehat{W}^{(k)} \right\|_F &\leq \theta \left\| Z^{(k)} - Z^{(k-1)} \right\|_F + \alpha \left\| X^{(k)} - X^{(k-1)} \right\|_F \\ &\quad + \widetilde{\beta} \left\| Z^{(k)} - Z^{(k-1)} \right\|_F \\ &\leq c \left\| W^{(k)} - W^{(k-1)} \right\|_F, \quad \forall k \geq 1, \end{aligned}$$

where  $c = \left( \theta + \alpha + \widetilde{\beta} \right)$  is a bounded positive constant. ■

*Theorem 3:* Suppose  $\{W^{(k)}\}$  to be a sequence obtained by the alternating proximal gradient Algorithm 1,  $W^{(k)} = \left( (X^{(k)})^T, (Z^{(k)})^T \right)^T$ ,  $\Omega$  being the set of the limit points of  $\{W^{(k)}\}$ , then,

- (1)  $\Omega$  is not empty and  $\Omega \subset \text{crit} \mathcal{Q}$ ;
- (2)  $\mathcal{Q}$  is a constant on  $\Omega$  and it is equal to  $\lim_{k \rightarrow \infty} \mathcal{Q} \left( W^{(k)} \right) = \inf_{k \in N} \mathcal{Q} \left( W^{(k)} \right)$ .

*Proof:* Since  $\mathcal{Q}$  is a coercive function and  $\mathcal{Q} \left( W^{(k)} \right)$  is nonincreasing,  $\{W^{(k)}\}$  must be a bounded sequence. By the classical properties of the bounded sequence,  $\Omega$  is a nonempty set.

For any  $X, Z \in \mathbb{R}^{s^2 \times t}$ , the formulations (11) and (12) imply that

$$\begin{aligned} \mathcal{Q} \left( X^{(k)}, Z^{(k-1)} \right) + \frac{\widetilde{\alpha}}{2} \left\| X^{(k)} - X^{(k-1)} \right\|_F^2 \\ \leq \mathcal{Q} \left( X, Z^{(k-1)} \right) + \frac{\widetilde{\alpha}}{2} \left\| X - X^{(k-1)} \right\|_F^2, \end{aligned}$$

and

$$\begin{aligned} \mathcal{Q} \left( X^{(k)}, Z^{(k)} \right) + \frac{\widetilde{\beta}}{2} \left\| Z^{(k)} - Z^{(k-1)} \right\|_F^2 \\ \leq \mathcal{Q} \left( X^{(k)}, Z \right) + \frac{\widetilde{\beta}}{2} \left\| Z - Z^{(k-1)} \right\|_F^2. \end{aligned}$$

Adding above two inequalities and setting  $Z = Z^{(k-1)}$ ,

$$\begin{aligned} \mathcal{Q} \left( X^{(k)}, Z^{(k)} \right) + \frac{\rho_{\min}}{2} \left\| W^{(k)} - W^{(k-1)} \right\|_F^2 \\ \leq \mathcal{Q} \left( X, Z^{(k-1)} \right) + \frac{\rho_{\max}}{2} \left\| X - X^{(k-1)} \right\|_F^2, \end{aligned} \quad (17)$$

where  $\rho_{\max}$  and  $\rho_{\min}$  are the maximum and minimum of  $\widetilde{\alpha}$  and  $\widetilde{\beta}$ . Assume  $W^* = \left( (X^*)^T, (Z^*)^T \right)^T$  to be a point in  $\Omega$ , then there must exist a subsequence  $\{W^{(k')}\}$  of  $\{W^{(k)}\}$  and  $\{W^{(k')}\}$  converges to  $W^*$ . By setting  $k = k'$  and  $X = X^*$  in (17),

$$\begin{aligned} \mathcal{Q} \left( X^{(k')}, Z^{(k')} \right) + \frac{\rho_{\min}}{2} \left\| W^{(k')} - W^{((k-1)')} \right\|_F^2 \\ \leq \mathcal{Q} \left( X^*, Z^{((k-1)')} \right) + \frac{\rho_{\max}}{2} \left\| X^* - X^{((k-1)')} \right\|_F^2. \end{aligned}$$

Since  $\mathcal{Q}$  is continuous about  $Z$ , then the above inequality implies

$$\liminf_{k' \rightarrow \infty} \mathcal{Q} \left( X^{(k')}, Z^{(k')} \right) \leq \mathcal{Q} \left( X^*, Z^* \right).$$

Owing to  $\mathcal{Q}$  is a lower semicontinuous function,

$$\liminf_{k' \rightarrow \infty} \mathcal{Q} \left( W^{(k')} \right) \geq \mathcal{Q} \left( X^*, Z^* \right).$$

Therefore,

$$\lim_{k' \rightarrow \infty} \mathcal{Q} \left( W^{(k')} \right) = \mathcal{Q} \left( X^*, Z^* \right) = \mathcal{Q} \left( W^* \right).$$

Suppose  $\widehat{W}^{(k')} = \left( \left( \widehat{X}^{(k')} \right)^T, \left( \widehat{Z}^{(k')} \right)^T \right)^T$  with  $\widehat{X}^{(k')}$  and  $\widehat{Z}^{(k')}$  as the same definition in that of Theorem 2, then,

$$\widehat{W}^{(k')} = \left( \left( \widehat{X}^{(k')} \right)^T, \left( \widehat{Z}^{(k')} \right)^T \right)^T \in \partial \mathcal{Q} \left( W^{(k')} \right),$$

and it follows by (10) and (14) that,

$$\lim_{k' \rightarrow \infty} \widehat{W}^{(k')} = \mathbf{0}.$$

Since  $\mathcal{Q} \left( W^* \right)$  is a closed set,  $\mathbf{0} \in \partial \mathcal{Q} \left( W^* \right)$ . Therefore,  $W^* \in \Omega$  is a critical point of  $\mathcal{Q}$  and  $\Omega \subset \text{crit} \mathcal{Q}$ .

For any point  $W^* \in \Omega$ , it has been proved that there must exist a subsequence  $\{W^{(k')}\}$  with  $\mathcal{Q} \left( W^{(k')} \right) \rightarrow \mathcal{Q} \left( W^* \right)$  as  $k' \rightarrow \infty$ . By the nonincreasing property of  $\mathcal{Q} \left( W^{(k)} \right)$ ,

$$\lim_{k \rightarrow \infty} \mathcal{Q} \left( W^{(k)} \right) = \inf_{k \in N} \mathcal{Q} \left( W^{(k)} \right) = \lim_{k' \rightarrow \infty} \mathcal{Q} \left( W^{(k')} \right). \quad \blacksquare$$

Since the matrix rank is a semialgebraic and Kurdyka-Łojasiewicz function [49]–[52]. The objective function  $\mathcal{Q}$  in (5) is the composition of finite Kurdyka-Łojasiewicz functions, and thus a Kurdyka-Łojasiewicz function [53], [54]. Based on Theorems 1-3 and Theorem 2.9 in [53], the global convergence of the alternating proximal gradient Algorithm 1 is as follows.

TABLE I  
THE DENOISED PSNRs FOR NOISE LEVEL  $\delta = 1$ .

Images	Method				
	TV	HTV	BM3D	WNNM	RM
Mon.	32.36	32.54	32.45	<b>33.91</b>	33.88
Boat	31.30	31.49	31.32	32.53	<b>32.54</b>
Bar.	31.16	31.15	33.65	34.04	<b>34.08</b>
Parrot	31.63	31.54	32.14	<b>32.86</b>	32.79
Villa	30.32	30.58	30.27	31.53	<b>31.76</b>
C.man	31.82	31.36	32.85	<b>33.75</b>	33.70
Plane	30.83	31.59	31.83	33.04	<b>33.08</b>
House	32.69	33.16	35.51	<b>35.89</b>	35.75
Baby	32.10	33.03	34.82	<b>35.24</b>	<b>35.24</b>
Pep.	32.52	30.75	33.61	33.85	<b>33.93</b>
Ave.	31.67	31.72	32.85	33.66	<b>33.67</b>

TABLE II  
THE DENOISED SSIMs FOR NOISE LEVEL  $\delta = 1$ .

Images	Method				
	TV	HTV	BM3D	WNNM	RM
Mon.	0.9149	0.9263	0.9453	<b>0.9525</b>	0.9518
Boat	0.8677	0.8857	0.8766	0.9009	<b>0.9016</b>
Bar.	0.8700	0.8768	0.9309	0.9339	<b>0.9354</b>
Parrot	0.8774	0.8976	0.8976	<b>0.9145</b>	0.9117
Villa	0.8096	0.8677	0.8800	0.9065	<b>0.9109</b>
C.man	0.8535	0.8735	0.9090	<b>0.9248</b>	0.9240
Plane	0.8096	0.8677	0.9120	0.9267	<b>0.9271</b>
House	0.8169	0.8465	0.8945	<b>0.9012</b>	0.8998
Baby	0.8227	0.8795	0.9456	0.9486	<b>0.9496</b>
Pep.	0.8786	0.8919	0.9149	0.9159	<b>0.9175</b>
Ave.	0.8521	0.8813	0.9106	0.9225	<b>0.9229</b>

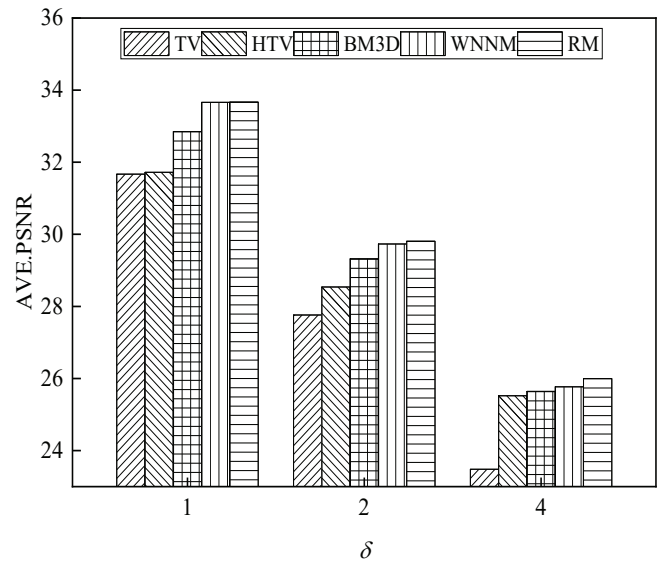
*Theorem 4:* Suppose  $\{W^{(k)}\}$  to be a sequence obtained by the alternating proximal gradient Algorithm 1,  $W^{(k)} = ((X^{(k)})^T, (Z^{(k)})^T)^T$ , then,  $\{W^{(k)}\}$  has finite length, i.e.,

$$\sum_{k=0}^{+\infty} \|W^{(k+1)} - W^{(k)}\|_F < +\infty,$$

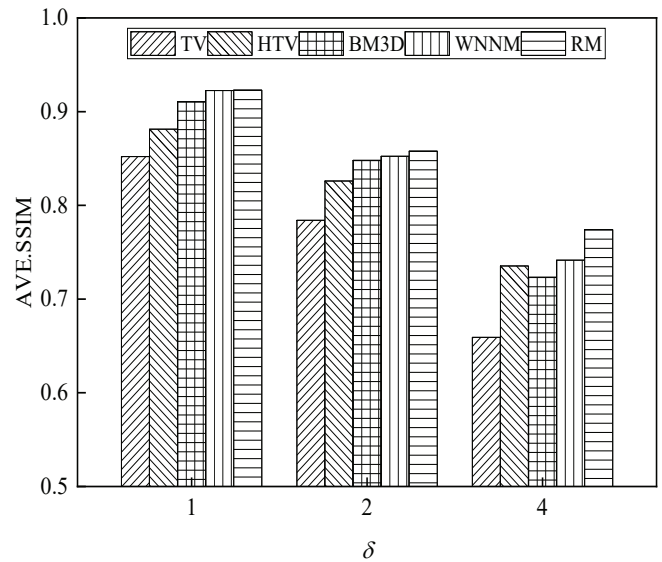
and  $\{W^{(k)}\}$  converges to a critical point of  $Q$ .

TABLE III  
THE DENOISED MAES FOR NOISE LEVEL  $\delta = 1$ .

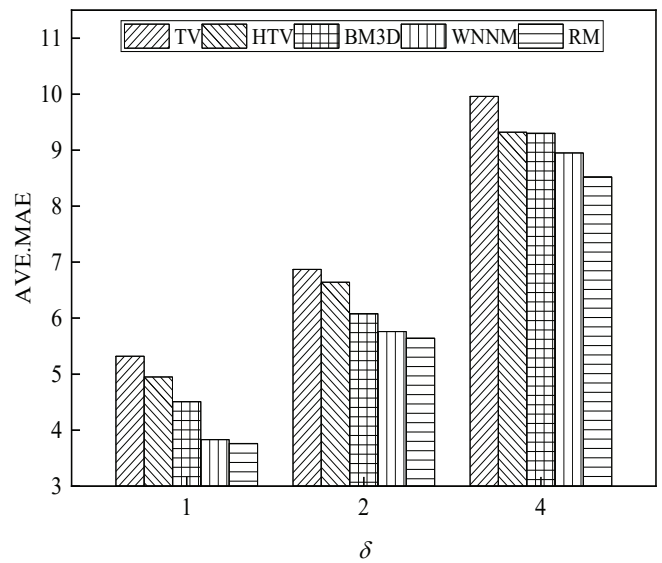
Images	Method				
	TV	HTV	BM3D	WNNM	RM
Mon.	5.21	4.66	4.88	3.75	<b>3.56</b>
Boat	6.26	6.04	5.80	4.56	<b>4.46</b>
Bar.	6.11	5.78	4.80	3.71	<b>3.69</b>
Parrot	5.32	5.26	5.18	3.98	<b>3.95</b>
Villa	6.41	5.66	5.27	4.97	<b>4.81</b>
C.man	5.13	4.72	4.64	3.56	<b>3.47</b>
Plane	5.11	5.00	4.24	3.99	<b>3.97</b>
House	4.01	3.95	3.13	3.03	<b>3.00</b>
Baby	4.79	3.68	3.45	2.97	<b>2.96</b>
Pep.	5.59	4.75	3.73	3.73	<b>3.69</b>
Ave.	5.32	4.95	4.51	3.83	<b>3.76</b>



(a)



(b)



(c)

Fig. 2. The histograms of recovered average measures: (a) PSNR, (b) SSIM, and (c) MAE by “TV”, “HTV”, “BM3D”, “WNNM” and our proposed “RM” methods, respectively.

TABLE IV  
THE DENOISED PSNRs FOR NOISE LEVEL  $\delta = 2$ .

Images	Method				
	TV	HTV	BM3D	WNNM	RM
Mon.	28.18	28.93	29.53	29.80	<b>29.84</b>
Boat	27.55	28.13	28.37	28.41	<b>28.70</b>
Bar.	27.83	28.28	29.36	<b>30.02</b>	29.92
Parrot	27.71	28.27	28.34	<b>28.63</b>	28.55
Villa	26.57	27.23	27.59	27.61	<b>28.01</b>
C.man	23.15	28.05	29.57	<b>29.72</b>	29.68
Plane	27.63	28.36	28.43	29.28	<b>29.30</b>
House	30.51	30.32	32.11	<b>32.83</b>	32.78
Baby	29.62	30.13	30.42	31.18	<b>31.34</b>
Pep.	28.87	27.65	29.43	29.86	<b>30.02</b>
Ave.	27.76	28.54	29.32	29.73	<b>29.81</b>

TABLE VII  
THE DENOISED PSNRs FOR NOISE LEVEL  $\delta = 4$ .

Images	Method				
	TV	HTV	BM3D	WNNM	RM
Mon.	22.47	25.27	25.40	25.27	<b>25.52</b>
Boat	23.86	24.92	24.99	25.02	<b>25.13</b>
Bar.	24.32	25.49	25.65	25.74	<b>25.90</b>
Parrot	23.47	25.37	24.83	24.88	<b>24.92</b>
Villa	23.50	24.17	23.94	23.95	<b>24.38</b>
C.man	19.35	25.23	25.49	25.69	<b>26.40</b>
Plane	20.61	25.17	25.00	25.19	<b>25.67</b>
House	26.58	27.49	28.26	28.49	<b>28.83</b>
Baby	25.84	27.23	27.07	27.08	<b>27.41</b>
Pep.	24.82	24.90	25.84	<b>26.40</b>	26.25
Ave.	23.48	25.52	25.64	25.77	<b>26.00</b>

TABLE V  
THE DENOISED SSIMs FOR NOISE LEVEL  $\delta = 2$ .

Images	Method				
	TV	HTV	BM3D	WNNM	RM
Mon.	0.8691	0.8846	0.9083	0.9040	<b>0.9053</b>
Boat	0.7673	0.7995	0.7942	0.7966	<b>0.8075</b>
Bar.	0.7927	0.8122	0.8460	<b>0.8561</b>	0.8546
Parrot	0.8168	0.8448	0.8289	<b>0.8410</b>	0.8365
Villa	0.7658	0.7968	0.8122	0.8101	<b>0.8251</b>
C.man	0.5261	0.8165	0.8534	0.8418	<b>0.8522</b>
Plane	0.8139	0.8185	0.8601	0.8753	<b>0.8763</b>
House	0.8142	0.7988	0.8472	<b>0.8593</b>	0.8587
Baby	0.8294	0.8437	0.8793	0.8789	<b>0.9001</b>
Pep.	0.8443	0.8448	0.8505	0.8604	<b>0.8617</b>
Ave.	0.7840	0.8260	0.8480	0.8524	<b>0.8578</b>

TABLE VIII  
THE DENOISED SSIMs FOR NOISE LEVEL  $\delta = 4$ .

Images	Method				
	TV	HTV	BM3D	WNNM	RM
Mon.	0.7122	0.7256	0.7896	0.8024	<b>0.8080</b>
Boat	0.5860	0.6698	0.6703	0.6713	<b>0.6742</b>
Bar.	0.6559	0.7251	0.7204	0.7115	<b>0.7329</b>
Parrot	0.6238	0.6875	0.7014	<b>0.7610</b>	0.7524
Villa	0.6438	0.7032	0.6652	0.6673	<b>0.7967</b>
C.man	0.4852	0.7715	0.6498	0.7762	<b>0.7828</b>
Plane	0.7252	0.7770	0.7576	0.7597	<b>0.7882</b>
House	0.7310	0.7844	0.7717	0.7965	<b>0.8059</b>
Baby	0.7432	0.8003	0.7610	0.7195	<b>0.8155</b>
Pep.	0.6852	0.6993	0.7453	0.7492	<b>0.7848</b>
Ave.	0.6592	0.7354	0.7232	0.7415	<b>0.7741</b>

TABLE VI  
THE DENOISED MAEs FOR NOISE LEVEL  $\delta = 2$ .

Images	Method				
	TV	HTV	BM3D	WNNM	RM
Mon.	6.90	6.50	6.42	5.61	<b>5.53</b>
Boat	7.67	7.84	7.21	6.83	<b>6.70</b>
Bar.	7.47	7.41	6.26	5.90	<b>5.89</b>
Parrot	6.97	6.67	6.37	6.16	<b>6.09</b>
Villa	8.47	8.35	7.32	7.29	<b>7.06</b>
C.man	6.68	6.49	5.72	5.34	<b>5.19</b>
Plane	7.21	6.73	6.13	6.12	<b>5.85</b>
House	5.19	5.10	4.45	4.05	<b>3.94</b>
Baby	5.77	5.13	5.11	4.84	<b>4.53</b>
Pep.	6.33	6.22	5.85	5.59	<b>5.48</b>
Ave.	6.87	6.64	6.08	5.76	<b>5.64</b>

TABLE IX  
THE DENOISED MAEs FOR NOISE LEVEL  $\delta = 4$ .

Images	Method				
	TV	HTV	BM3D	WNNM	RM
Mon.	10.87	9.65	9.37	9.40	<b>8.99</b>
Boat	10.85	10.39	10.28	10.17	<b>10.06</b>
Bar.	10.63	9.72	9.60	9.61	<b>9.23</b>
Parrot	9.94	9.83	9.65	9.78	<b>9.18</b>
Villa	11.82	11.13	11.08	11.15	<b>10.66</b>
C.man	9.36	8.70	8.97	7.53	<b>7.36</b>
Plane	10.44	9.49	9.46	9.26	<b>8.95</b>
House	8.00	7.55	6.82	6.07	<b>5.57</b>
Baby	8.32	7.67	7.82	7.99	<b>7.06</b>
Pep.	9.32	9.03	8.91	8.53	<b>8.17</b>
Ave.	9.96	9.32	9.30	8.95	<b>8.52</b>

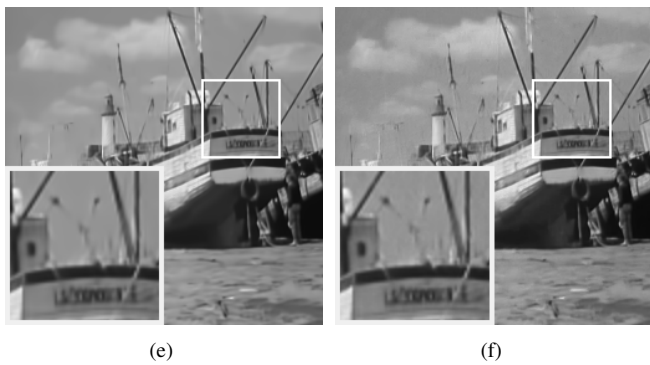
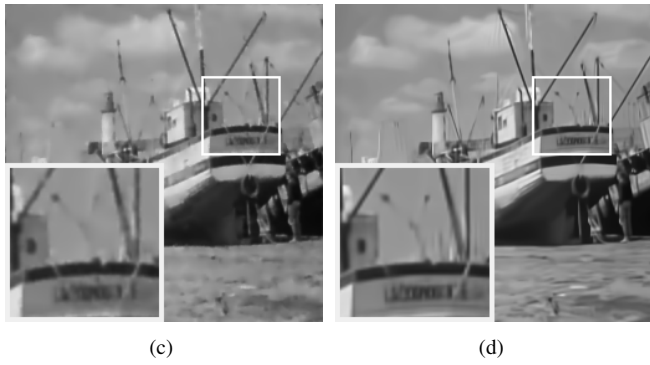
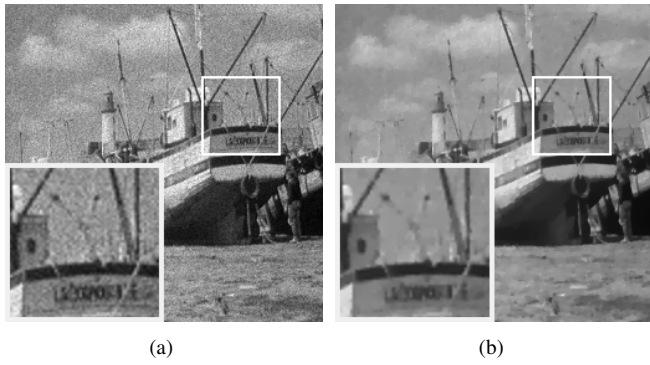


Fig. 3. Denoised results of Boat image for noise level  $\delta = 1$ ; (a) noisy image, (b)-(f) denoised images by “TV”, “HTV”, “BM3D”, “WNNM” and our proposed “RM” methods, respectively.

## V. NUMERICAL RESULTS

In this section, numerical experiments on both clean image simulation and real ultrasound image denoising are presented to illustrate the performance of the proposed method. For clean image simulation, ten constantly used 256-by-256 images adopted in the experiments are shown in Fig. 1. They are Monarch, Barbara, Villa, Plane, Baby in the left column, and Boat, Parrot, Cameraman, House, Peppers, in the right column, respectively. Three different levels of Gaussian noises with standard deviation  $\delta = 1, 2, 4$  are considered based on image degradation model (1).

To evaluate the image denoising performances, peak signal-to-noise ratio (PSNR), structural similarity index (SSIM) [55], and mean absolute-deviation error (MAE) are used as quantitative measurements. For a  $m$ -by- $n$  clean image  $f$ , the PSNR and MAE of its denoised image  $\hat{f}$  are calculate by formulations  $\text{PSNR} = 10 \log_{10} \frac{mn \cdot |\max(f) - \min(f)|^2}{\|\hat{f} - f\|_2^2}$  (dB) and  $\text{MAE} = \frac{\|\hat{f} - f\|_1}{mn}$ , respectively. Five excellent denoising methods including total

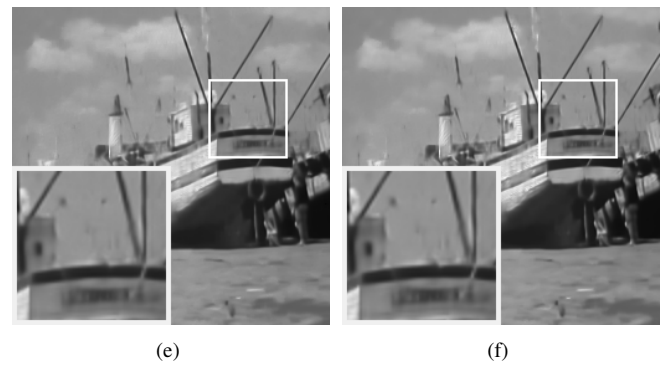
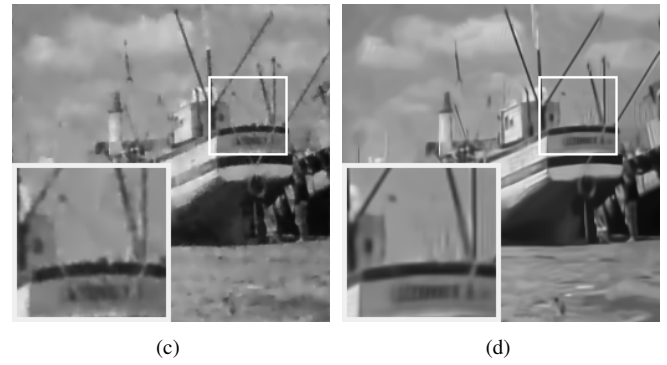
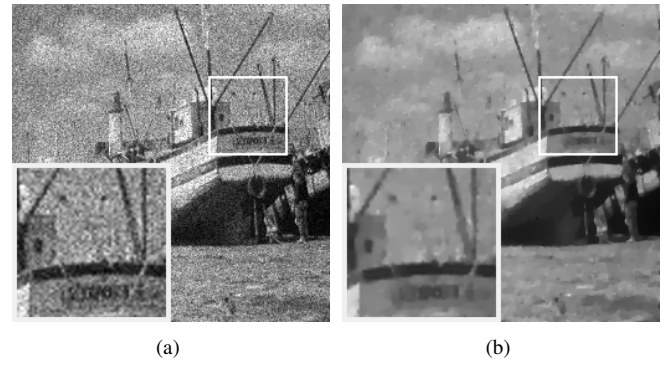


Fig. 4. Denoised results of Boat image for noise level  $\delta = 2$ ; (a) noisy image, (b)-(f) denoised images by “TV”, “HTV”, “BM3D”, “WNNM” and our proposed “RM” methods, respectively.

variation method “TV” [27], high-order TV method “HTV” [33], block matching and 3D filtering method “BM3D” [38], and patch-based weighted nuclear norm minimization method “WNNM” [44] are also conducted in the experiments to make comparisons.

### A. Image Denoising Algorithm and Parameters

Suppose the noisy image is divided into  $p$  overlapped reference patches, and there are subsequently formed  $p$  patch matching matrices  $Y_1, Y_2, \dots, Y_p$ . By adopting model (4) and its alternating proximal gradient algorithm to denoise each matrix  $Y_\zeta$  ( $\zeta = 1, 2, \dots, p$ ), a noise clean image  $\hat{f}$  can be recovered by rearranging the corresponding denoised image patches into an image. By introducing an iteration scheme to update  $Y_1, Y_2, \dots, Y_p$  from the latest iteration denoised image  $\hat{f}$ , the residue noises existed in  $\hat{f}$  can be finally removed. The whole image denoising method is included in Algorithm 2.

In Algorithm 2, the image block matching schemes [4], [5] are adopted to construct the patch matching matrices  $Y_\zeta$

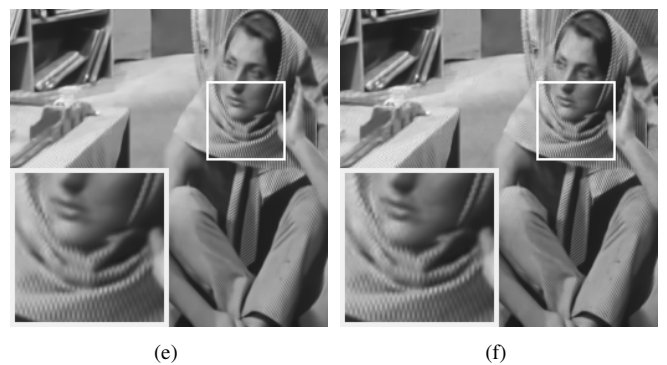
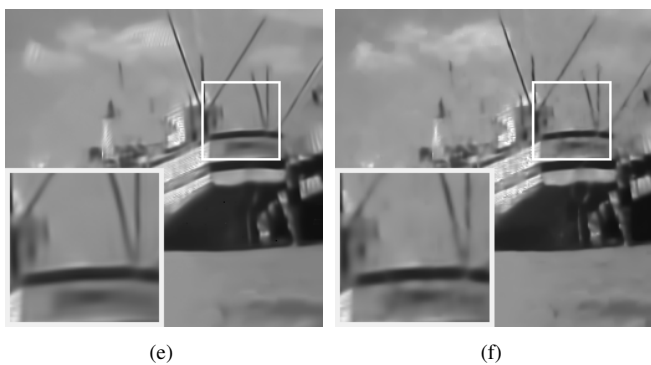
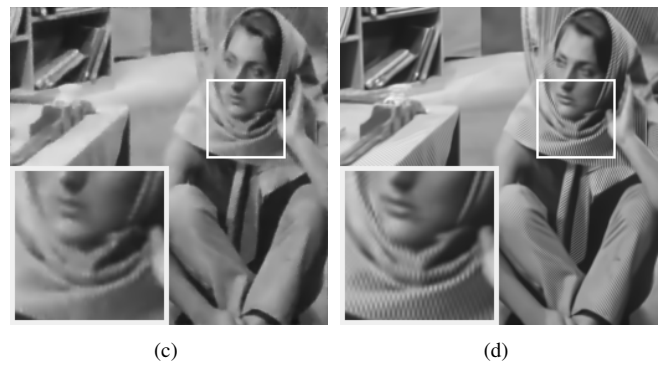
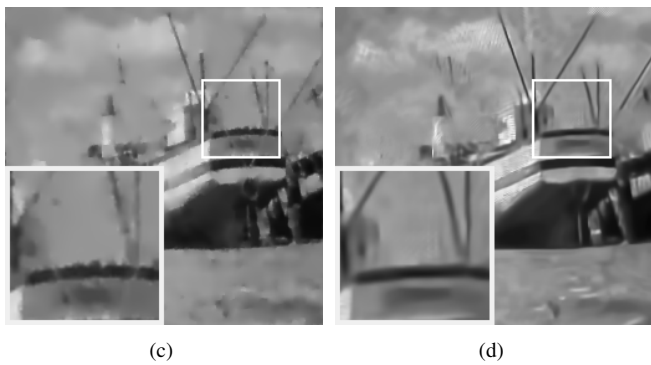
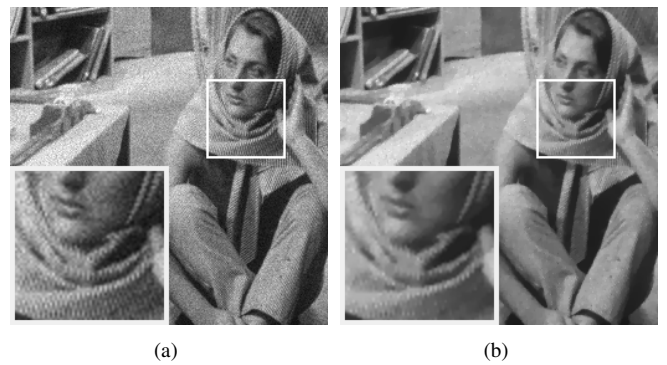
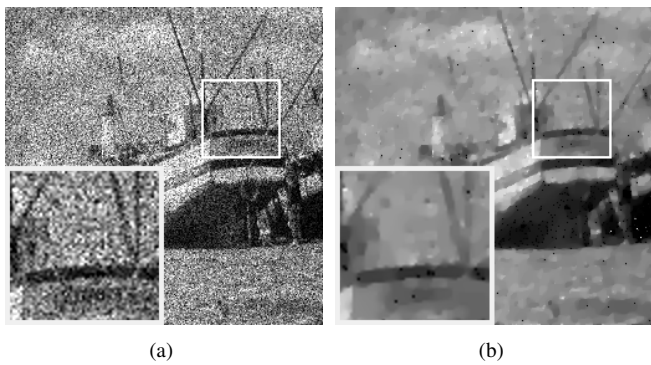


Fig. 5. Denoised results of Boat image for noise level  $\delta = 4$ ; (a) noisy image, (b)-(f) denoised images by “TV”, “HTV”, “BM3D”, “WNNM” and our proposed “RM” methods, respectively.

Fig. 6. Denoised results of Barbara image for noise level  $\delta = 1$ ; (a) noisy image, (b)-(f) denoised images by “TV”, “HTV”, “BM3D”, “WNNM” and our proposed “RM” methods, respectively.

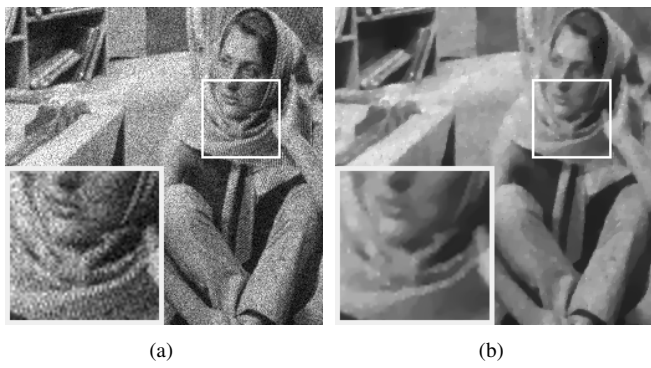
( $\zeta = 1, 2, \dots, p$ ). The similarity between a reference patch and its similar patches measured by the matrix Frobenius norm, reference to [44], [47]. The size of reference patch is considered as 6-by-6 and its 70 most similar patches are used to aggregate the patch matching matrix, namely,  $s = 6$  and  $t = 70$ .  $\theta$  is a penalty parameter in model (5) and its selection depends on the different noise levels. For noise levels  $\sigma = 1$ ,  $\sigma = 2$ , and  $\sigma = 4$ , the optimal value of  $\theta$  are selected as 10, 15, and 25 respectively. By the same consideration introduced in [40], [44], [47], [56],  $\omega = 2\sqrt{2t\delta^2}$  and where  $\delta$  represents the estimated noise variance of the image. The parameters  $\alpha, \beta$  is selected as  $\theta + 10^{-5}$  and  $K$  is selected as 25. Parameters in five compared methods are selected as those suggested by their authors, or to obtain the best image denoising quantitative measurements.

### B. Image Denoising Results

The PSNR, SSIM, and MAE measures of all denoised images are shown in Tables I-III, Tables IV-VI, Tables VII-IX with respect to different noise levels  $\delta = 1$ ,  $\delta = 2$

and  $\delta = 4$ , respectively. The best denoised measures for each image recovery are shown in boldface in these tables. Clearly, the “WNNM” method and our proposed “RM” method obtained all of the best denoised measures. The proposed “RM” method obtain most of the best PSNRs and SSIMs, and all of the best MAEs in these tables. The average PSNRs, SSIMs, and MAEs of all tested images with respect to different noise levels  $\delta = 1$ ,  $\delta = 2$  and  $\delta = 4$  are shown in the last line of each Table. The best average PSNRs, SSIMs, and MAEs are shown in boldface and they all obtained by our proposed “RM” method for different noise levels  $\delta = 1$ ,  $\delta = 2$  and  $\delta = 4$ . Specifically, for noise level  $\delta = 4$ , the proposed “RM” method outperform the “TV”, “HTV”, “BM3D” and “WNNM” methods on best average PSNR, SSIM and MAE by significant margins 2.52, 0.48, 0.36, 0.23 (dB), 0.1149, 0.0387, 0.0509, 0.0326, and 1.44, 0.80, 0.78, 0.43, respectively. Moreover, the histograms of these average PSNRs, SSIMs, and MAEs are shown in Fig. 2.

In addition to PSNR, SSIM and MAE evaluations, the



(a)

(b)



(c)

(d)



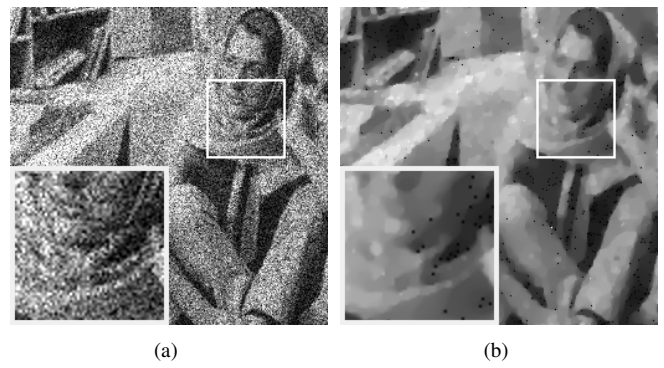
(e)

(f)

Fig. 7. Denoised results of Barbara image for noise level  $\delta = 2$ ; (a) noisy image, (b)-(f) denoised images by “TV”, “HTV”, “BM3D”, “WNNM” and our proposed “RM” methods, respectively.

denoised Boat, Barbara, Plane, and Baby images are shown respectively in Figs. 3-5, Figs. 6-8, Figs. 9-11 and Figs. 12-14 to make a comparison of the visual qualities. In these figures, the images denoised by patch-based “BM3D”, “WNNM” and our proposed “RM” methods exhibit significant better visual effects compared to those denoised by “TV” and “HTV” methods. To check the recovered details, we encircle one small block with a white square box and then show it in an enlarged version in each image in these figures. From these enlarged blocks, it is shown that the denoised images by proposed “RM” method have slightly better visual effects than those denoised by excellent “BM3D” and “WNNM” methods. For instance, the enlarged blocks in “RM” method recovered Plane images in Figs. 9-11 and Baby images in Figs. 12-14 are shown clearly more details than those in images recovered by “BM3D” and “WNNM” methods.

For the computational time, the nonlocal low-rank prior-based “WNNM” and our proposed “RM” methods require much longer time. Since their image blocking matching schemes and SVD-based image denoising operations are



(a)

(b)



(c)

(d)



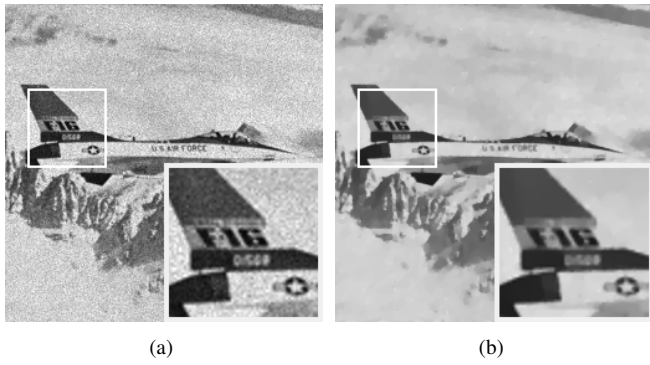
(e)

(f)

Fig. 8. Denoised results of Barbara image for noise level  $\delta = 4$ ; (a) noisy image, (b)-(f) denoised images by “TV”, “HTV”, “BM3D”, “WNNM” and our proposed “RM” methods, respectively.

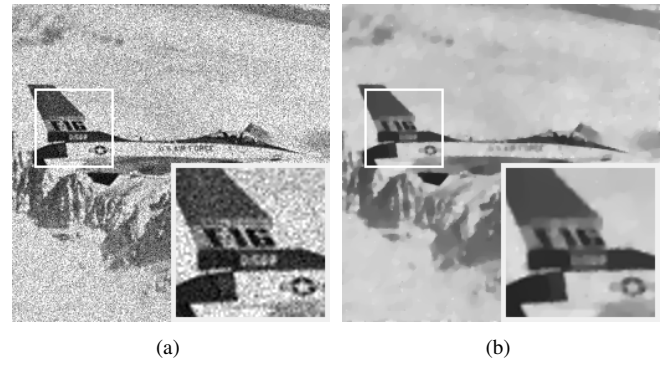
more time consuming, see, [40], [44], [47].

The experiments on denoising of two real ultrasound images are also conducted to show the effects of our proposed method. The real noisy images and their denoised images by methods “TV”, “HTV”, “BM3D”, “WNNM” and “RM” are shown in Figs. 15-16, respectively. In figures, the left column lists the noisy image and its denoised versions by different methods; the right column lists the enlarged versions of small blocks, marked in the left column images by a white box, to show the details of those denoised images more clearly. From these figures, we can see that the recovered images of “TV” and “HTV” methods are over smoothed, and the recovered images of “BM3D”, “WNNM” and our proposed “RM” methods obtain better visual effects. The “HTV”, “BM3D” and “WNNM” methods are all current state-of-the-art methods for ultrasound image denoising. The above numerical results on clean image simulation and real ultrasound image denoising illustrate that the proposed “RM” method can perform better than those excellent methods for speckle noise removal in ultrasound images.



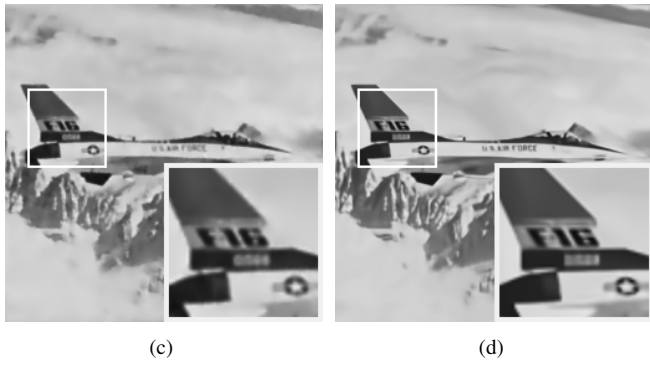
(a)

(b)



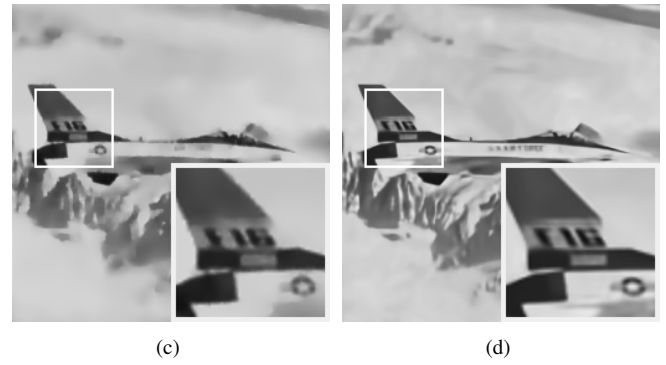
(a)

(b)



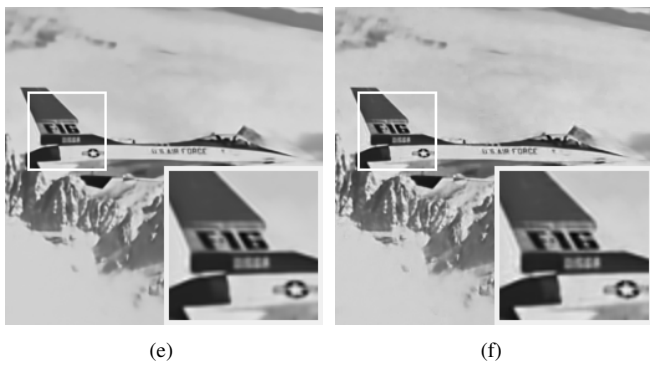
(c)

(d)



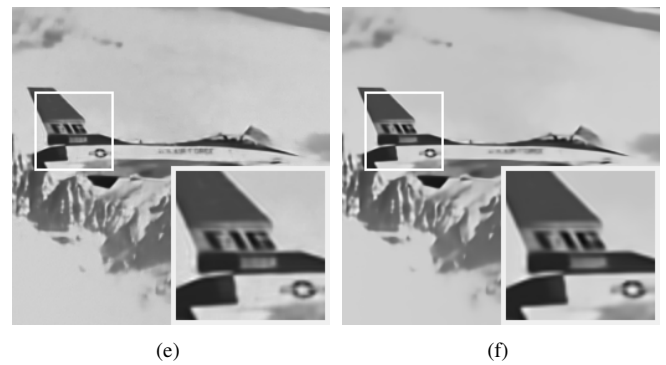
(c)

(d)



(e)

(f)



(e)

(f)

Fig. 9. Denoised results of Plane image for noise level  $\delta = 1$ ; (a) noisy image, (b)-(f) denoised images by “TV”, “HTV”, “BM3D”, “WNNM” and our proposed “RM” methods, respectively.

Fig. 10. Denoised results of Plane image for noise level  $\delta = 2$ ; (a) noisy image, (b)-(f) denoised images by “TV”, “HTV”, “BM3D”, “WNNM” and our proposed “RM” methods, respectively.

## VI. CONCLUSION

In this paper, we develop a novel LRM-based method for ultrasound image denoising. Taking advantage of image nonlocal similarities, we firstly propose a matrix rank minimization model for speckle noise removal. Then, we design an alternating proximal gradient method to the non-convex and nonsmooth rank minimization model. The global convergence theory of the algorithm is well analyzed. By adopting the proposed speckle noise removal model and its solving algorithm, we finally establish an ultrasound noise reduction method. Numerical experiments show that the proposed matrix rank minimization-based method can well compete with the current start-of-art methods for ultrasound image denoising.

## REFERENCES

- [1] R. Gonzalez and R. Woods, *Digital Image Processing (3rd edition)*, Pearson International Edition, Prentice Hall, 2008.
- [2] G. Cristóbal, P. Schelkens and H. Thienpont, *Optical and Digital Image Processing*, John Wiley & Sons, 2013.
- [3] L. Rudin, S. Osher and E. Fatemi, “Nonlinear total variation based noise removal algorithms,” *Physica D: Nonlinear Phenomena*, vol. 60, no.1-4, pp. 259–268, 1992.
- [4] A. Buades, B. Coll and J. M. Morel, “A review of image denoising algorithms, with a new one,” *Multiscale Model. Simul.* vol. 4, no. 2, pp. 490–530, 2005.
- [5] A. Buades, B. Coll and J. M. Morel, “A non-local algorithm for image denoising,” in *IEEE Conf. Comput. Vision and Pattern Recognit. (CVPR) 2005*, pp. 60–65.
- [6] M. Elad and M. Aharon, “Image denoising via sparse and redundant representations over learned dictionaries,” *IEEE Trans. Image Process.* vol. 15, no. 12, pp. 3736–3745, 2006.
- [7] K. Dabov, A. Foi V. Katkovnik and K. Egiazarian, “Image denoising by sparse 3-D transform-domain collaborative filtering,” *IEEE Trans. Image Process.* vol. 16, no. 8, pp. 2080–2095, 2007.
- [8] A. K. Awasthi, Y. Kumar and H. Abdullahi, “Optimizing conjugate gradient directions for image deblurring in compressed sensing: a hybridized approach,” *IAENG International Journal of Applied Mathematics.* vol. 54, no. 11, pp. 2500–2511, 2024.
- [9] S. A. Kassam, *Signal Detection in Non-Gaussian Noise*, Springer Science Business Media, Berlin, 2012.
- [10] D. Guan, D. Xiang, X. Tang and G. Kuang, “SAR image despeckling based on nonlocal low-rank regularization,” *IEEE Trans. Geosci. Remote* vol. 57, no. 6, pp. 3472–3489, 2019.
- [11] C. Brune, A. Sawatzky and M. Burger, “Primal and dual Bregman methods with application to optical nanoscopy,” *Int. J. Comput. Vis.* vol. 92, pp. 211–229, 2011.

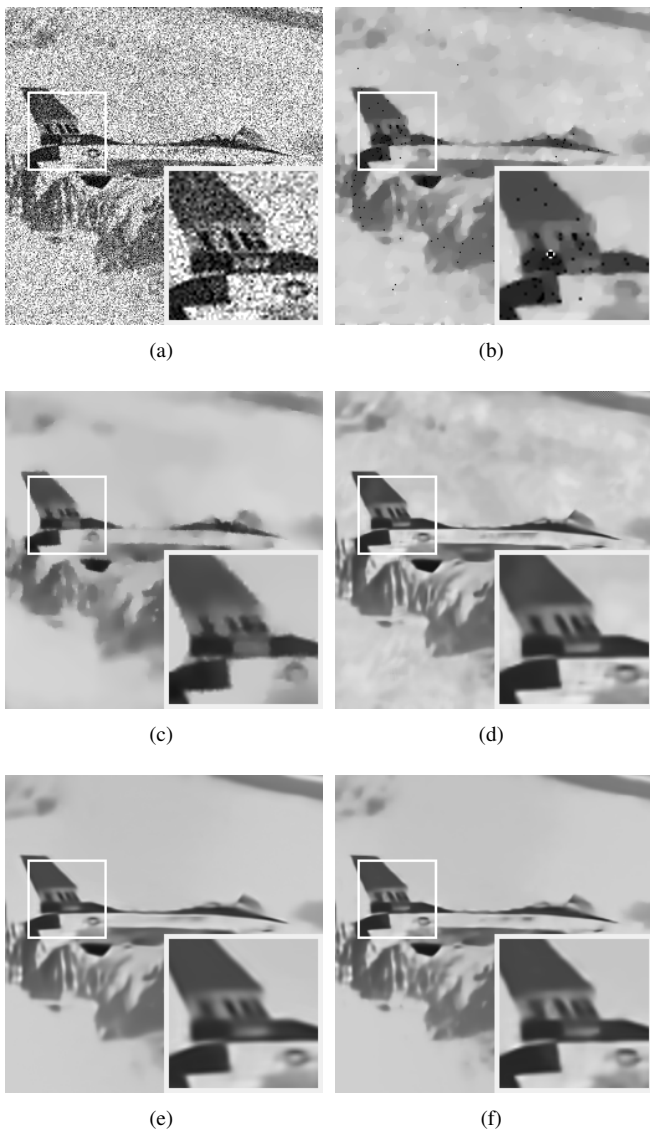


Fig. 11. Denoised results of Plane image for noise level  $\delta = 4$ ; (a) noisy image, (b)-(f) denoised images by “TV”, “HTV”, “BM3D”, “WNNM” and our proposed “RM” methods, respectively.

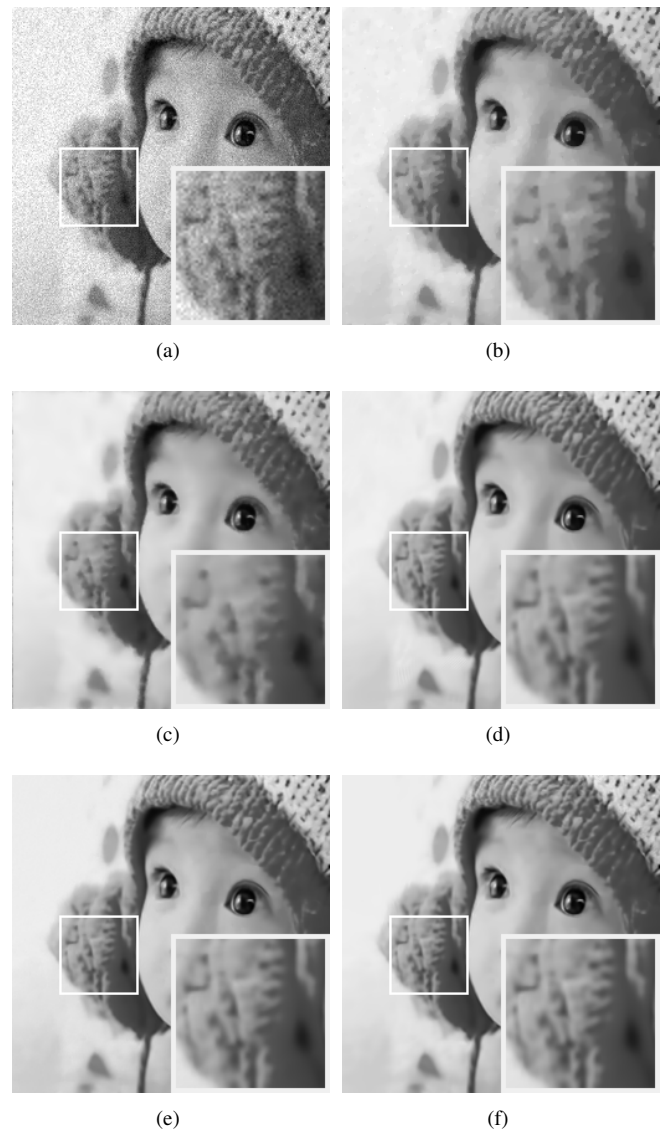


Fig. 12. Denoised results of Baby image for noise level  $\delta = 1$ ; (a) noisy image, (b)-(f) denoised images by “TV”, “HTV”, “BM3D”, “WNNM” and our proposed “RM” methods, respectively.

[12] H.-Y. Yan and Y.-M. Huang, “Cauchy noise removal by a generalized nonlocal low-rank method,” *SPIE J. Electron. Imaging* vol. 31, no. 3, 033022, 2022.

[13] D. Yi, Z. You and W. Zhang, “Image enhancement CHPSO processing technology based on improved particle swarm optimization algorithm,” *IAENG International Journal of Computer Science*. vol. 52, no. 1, pp. 130–142, 2025.

[14] W. Du, X. Ouyang, N. Zhao and Y. Ouyang, “BCS-YOLOv8s: a detecting method for dense small targets in remote sensing images based on improved YOLOv8s,” *IAENG International Journal of Computer Science*. vol. 52, no. 2, pp. 417–426, 2025.

[15] M. Zhao, Y.-W. Wen and M. Ng, “A nonlocal low rank model for poisson noise removal,” *Inverse Problems Imaging* vol. 15, no. 3, pp. 519, 2021.

[16] V. Damerjian, O. Tankyevych, N. Souag and E. Petit, “Speckle characterization methods in ultrasound images-A review,” *J. Amer. Math. Soc.* vol. 35, pp. 202–213, 2014.

[17] W. Feng, H. Lei and Y. Gao, “Speckle reduction via higher order total variation approach,” *IEEE Trans. Image Process.* vol. 23, no. 4, pp. 1831–1843, 2014.

[18] Y. G. Wang, L. Wang and Y. X. Geng, “Research on medical image classification based on triple fusion attention,” *Engineering Letters*. vol. 33, no. 1, pp. 124–131, 2025.

[19] J. S. Lee, “Digital image enhancement and noise filtering by use of local statistics,” *IEEE Trans. Pattern Anal. Mach. Intell.* vol. 2, no. 2, pp. 165–168, 1980.

[20] V. S. Frost, J. A. Stiles, K. S. Shanmugan and J. C. Holtzman, “A

model for radar images and its application to adaptive digital filtering of multiplicative noise,” *IEEE Trans. Pattern Anal. Mach. Intell.* vol. 4, no. 2, pp. 157–166, 1982.

[21] T. Loupas, W. McDicken and P. Allan, “An adaptive weighted median filter for speckle suppression in medical ultrasonic images,” *IEEE Trans. Circuits Syst.* vol. 36, pp. 129–135, 1989.

[22] A. Achim, P. Tsakalides and A. Bezerianos, “SAR image denoising via Bayesian wavelet shrinkage based on heavy-tailed modeling,” *IEEE Trans. Geosci. Remote Sens.* vol. 41, no. 8, pp. 1773–1784, 2003.

[23] T. Bianchi, F. Argenti and L. Alparone, “Segmentation-based MAP despeckling of SAR images in the undecimated wavelet domain,” *IEEE Trans. Geosci. Remote Sens.* vol. 46, no. 9, pp. 2728–2742, 2008.

[24] S. Ge, D. Liu, X. Shi, X. Zhao, X. Wang and J. Fan, “Semantic segmentation of remote sensing images based on filtered hybrid attention mechanisms,” *Engineering Letters*. vol. 33, no. 1, pp.80–89, 2025.

[25] L. Rudin, P. Lions and S. Osher, *Multiplicative Denoising and Deblurring: Theory and Algorithms, Geometric Level Sets in Imaging, Vision, and Graphics*. Springer, 2003.

[26] G. Aubert and J. F. Aujol, “A variational approach to removing multiplicative noise,” *SIAM J. Appl. Math.* vol. 68, no. 4, pp. 925–946, 2008.

[27] Z. Jin and X. Yang, “A variational model to remove the multiplicative noise in ultrasound images,” *J. Math. Imag. Vision* vol.39, no. 1, pp. 62–74, 2011.

[28] J. Huang and X. Yang “Fast reduction of speckle noise in real ultrasound images,” *Signal Process.* vol. 93, no. 4, pp. 684–694, 2013.

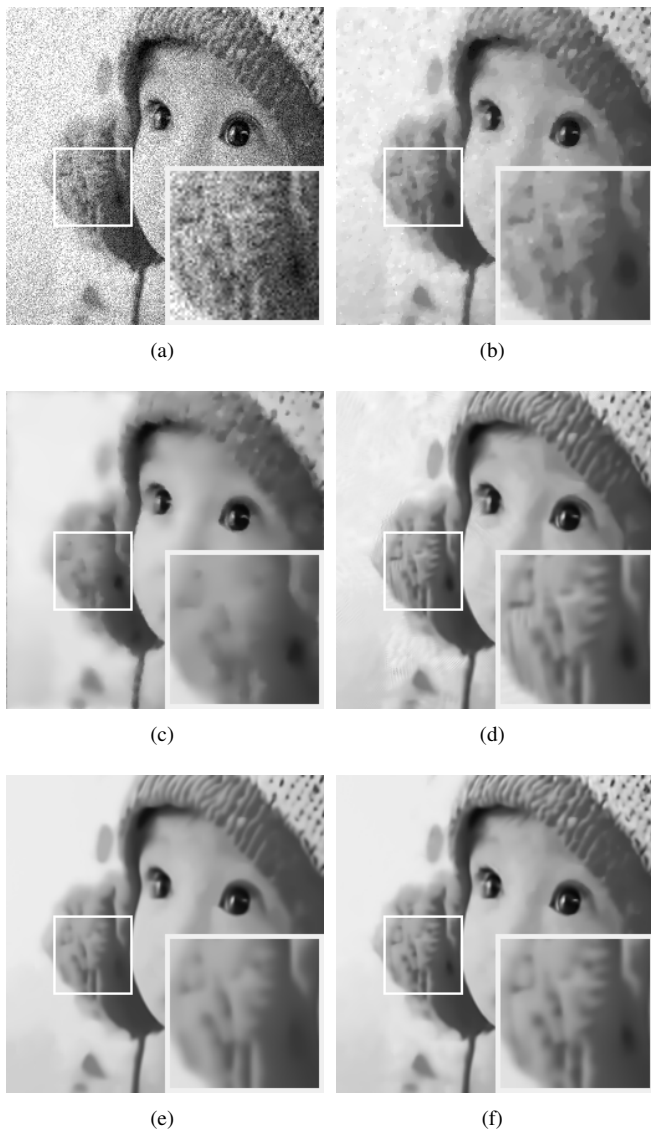


Fig. 13. Denoised results of Baby image for noise level  $\delta = 2$ ; (a) noisy image, (b)-(f) denoised images by “TV”, “HTV”, “BM3D”, “WNNM” and our proposed “RM” methods, respectively.

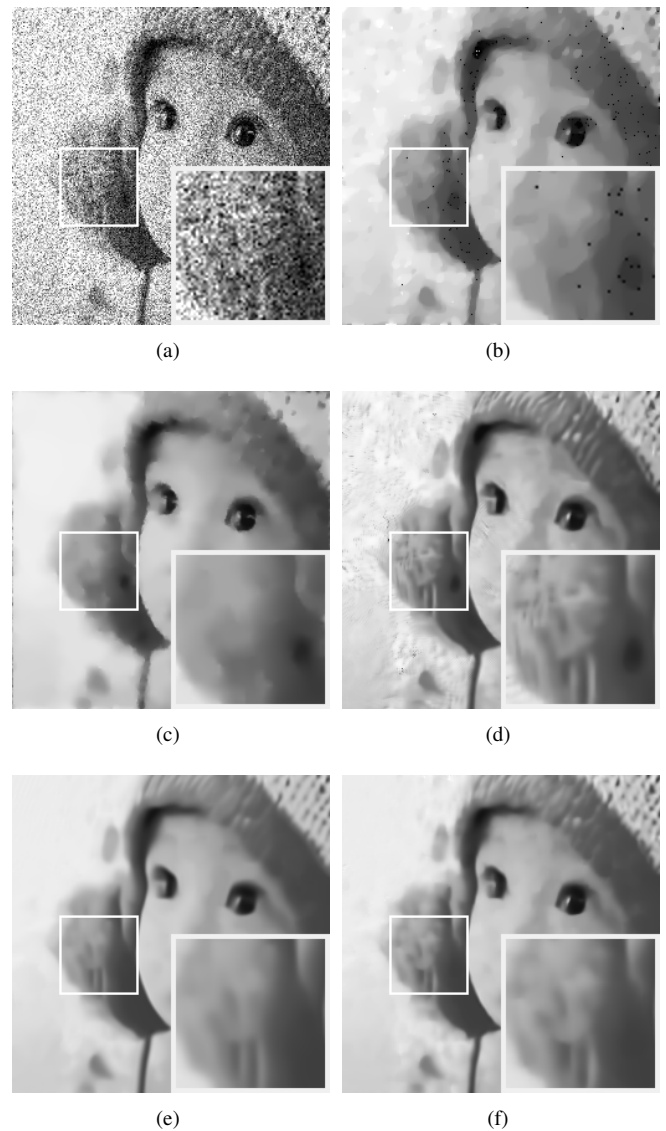


Fig. 14. Denoised results of Baby image for noise level  $\delta = 4$ ; (a) noisy image, (b)-(f) denoised images by “TV”, “HTV”, “BM3D”, “WNNM” and our proposed “RM” methods, respectively.

[29] Y. Wu and X. Feng, “Speckle noise reduction via nonconvex high total variation approach,” *Math. Problems Eng.* vol. 2, pp. 1–11, 2015.

[30] T. Surya Kavitha, A. Vamsidhar, G. Sunil Kumar, R. Viswanadham, V. Anand Kumar and T. Madhuri, “Underwater image enhancement using fusion of CLAHE and total generalized variation,” *Engineering Letters*. vol. 31, no. 4, pp. 1724-1739, 2023.

[31] M. Kang and M. Jung, “Total generalized variation based denoising models for ultrasound images,” *J. Sci. Comput.* vol. 72, no. 1, pp. 172–197, 2017.

[32] J.-J. Mei, T.-Z. Huang, S. Wang and X.-L. Zhao, “Second order total generalized variation for speckle reduction in ultrasound images,” *J. Franklin Institute* vol. 355, pp. 574–595, 2018.

[33] S. Wang, T.-Z. Huang, X.-L. Zhao, J.-J. Mei and J. Huang, “Speckle noise removal in ultrasound images by first-and second-order total variation,” *Numer. Algorithms* vol. 78, pp. 513–533, 2018.

[34] B. A. Abraham and Y. Kanah “Speckle noise reduction method combining total variation and wavelet shrinkage for clinical ultrasound imaging,” *IEEE Middle East Conference on Biomedical Engineering* pp. 80–83, 2011.

[35] H. Ji, C. Liu, Z. Shen and Y. Xu, “Robust video denoising using low-rank matrix completion,” *IEEE Conf. Comput. Vision and Pattern Recognit. (CVPR)*, pp. 1791–1798, 2010.

[36] M. Ma, “Color image restoration via quaternion-based hybrid regularization method,” *IAENG International Journal of Applied Mathematics*. vol. 54, no. 11, pp. 2176-2182, 2024.

[37] C. Xu, “Adaptive total variation regularization for weighted low-rank

tensor sparse hyperspectral unmixing,” *IAENG International Journal of Applied Mathematics*. vol. 54, no. 11, pp. 2404-2417, 2024.

[38] Y. Gan, E. Angelint, A.Laine and C. Hendon, “BM3D-based ultrasound image denoising via brushlet thresholding,” in *IEEE 12th International Symposium on Biomedical Imaging 2015* pp. 667–670.

[39] M. Fazel, H. Hindi and S. P. Boyd, “A rank minimization heuristic with application to minimum order system approximation,” in *Proceedings of the American Control Conference 2001*, pp. 4734–4739.

[40] S. Gu, L. Zhang, W. Zuo and X. Feng, “Weighted nuclear norm minimization with application to image denoising,” in *IEEE Conf. Comput. Vision and Pattern Recognit. (CVPR) 2014*, pp. 2862–2867.

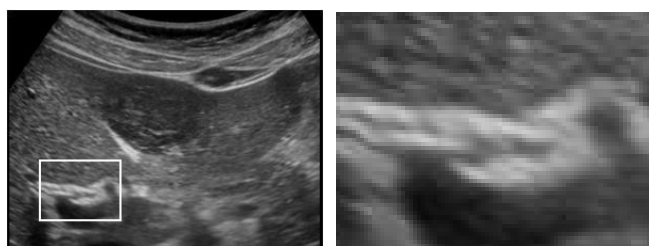
[41] S. Gu, Q. Xie, D. Meng, W. Zuo, X. Feng and L. Zhang, “Weighted nuclear norm minimization and its applications to low level vision,” *International Journal of Computer Vision* vol. 121, pp. 183–208, 2017.

[42] Y.-M. Huang and H.-Y. Yan, “Weighted nuclear norm minimization based-regularization method for image restoration,” *Commun. Appl. Math Comput.* vol. 3, no. 3, pp. 371–389, 2021.

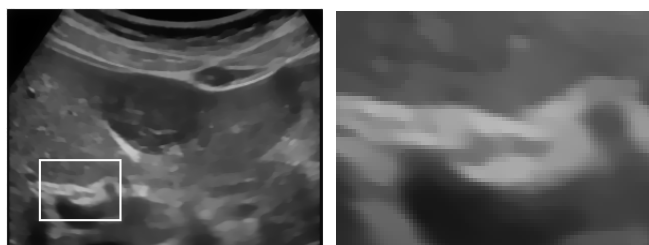
[43] X. Liu, J. Lu, L. Shen, C. Xu and Y. Xu, “Multiplicative noise removal: ronlocal low-rank rodel and its proximal alternating reweighted minimization algorithm,” *SIAM J. Imag. Sci.* vol. 13, no. 3, pp. 1595–1629, 2020.

[44] X. G. Lv, F. Li, J. Liu and S. T. Lu, “A patch-based low-rank minimization approach for speckle noise reduction in ultrasound images,” *Adv. Appl. Math. Mech.* vol. 14, no. 1, pp. 155–180, 2022.

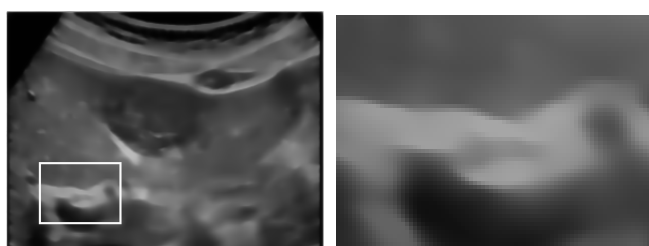
[45] F. Bo, W. Lu, G. Wang, M. Zhou, Q. Wang and J. Fang “A blind SAR image despeckling method based on improved weighted nuclear



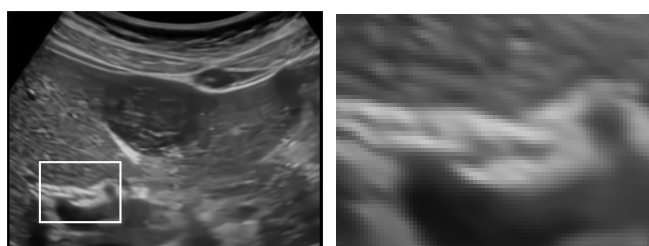
(a) (b)



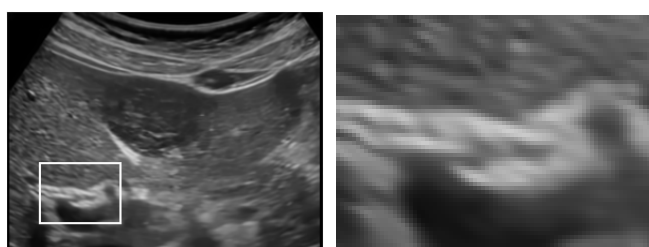
(c) (d)



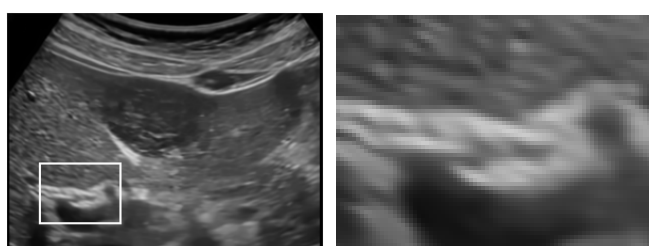
(e) (f)



(g) (h)

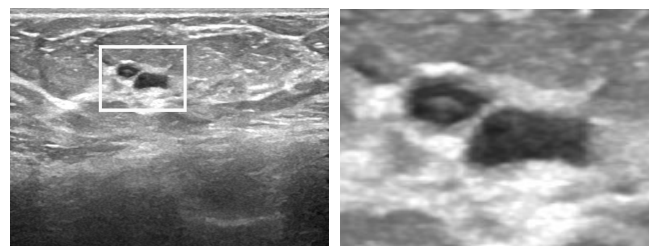


(i) (j)

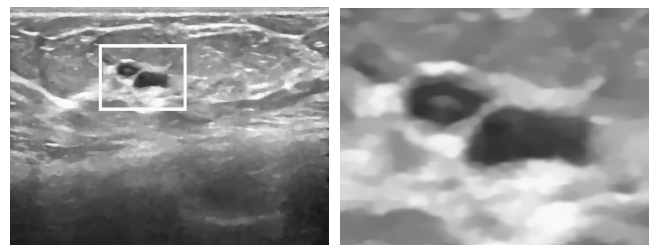


(k) (l)

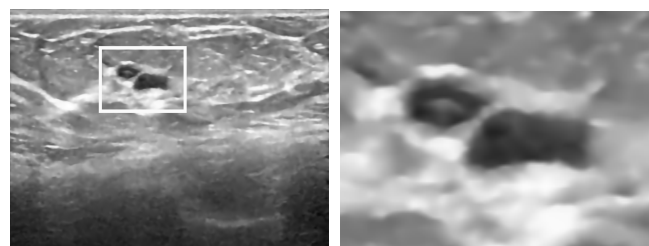
Fig. 15. Image denoising results for the first real ultrasound image; (a) the noisy image, (c), (e), (g), (i), (k) are its denoised images by “TV”, “HTV”, “BM3D”, “WNNM” and the proposed “RM” methods; (b), (d), (f), (h), (j), (l) are the enlarged versions of small blocks marked in (a), (c), (e), (g), (i), (k) images; respectively.



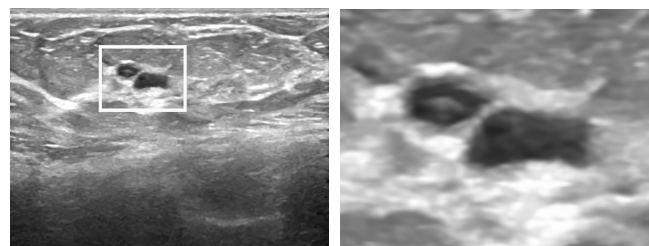
(a) (b)



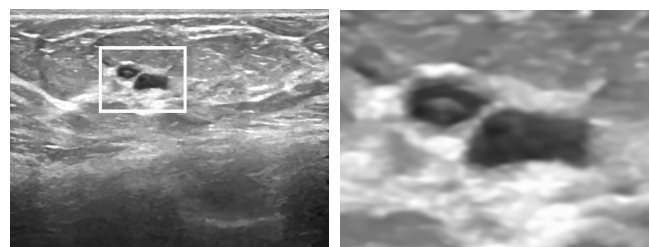
(c) (d)



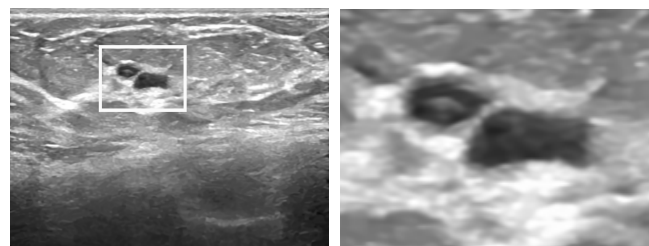
(e) (f)



(g) (h)



(i) (j)



(k) (l)

Fig. 16. Image denoising results for the second real ultrasound image; (a) the noisy image, (c), (e), (g), (i), (k) are its denoised images by “TV”, “HTV”, “BM3D”, “WNNM” and the proposed “RM” methods; (b), (d), (f), (h), (j), (l) are the enlarged versions of small blocks marked in (a), (c), (e), (g), (i), (k) images; respectively.

- norm minimization," *IEEE Geosci. Remote Sens. Lett.* vol. 19, pp. 1–5, 2022.
- [46] H. Yang, J. Lu, Y. Luo, G. Zhang, H. Zhang, Y. Liang and J. Lu, "Nonlocal ultrasound image despeckling via improved statistics and rank constraint," *Pattern Anal. Appl.* vol. 26, no. 1, pp. 217–237, 2023.
- [47] Y.-M. Huang, H.-Y. Yan, Y.-W. Wen and X. Yang, "Rank minimization with applications to image noise removal," *Inform. Sciences* vol. 429, pp. 147–163, 2018.
- [48] B. Mordukhovich, *Variational Analysis and Generalized Differentiation. I. Basic Theory*, Grundlehren der Mathematischen Wissenschaften, Springer-Verlag, Berlin, (2006).
- [49] H.-Y. Yan, "Nonlocal matrix rank minimization method for multiplicative noise removal," *Commun. Appl. Math Comput.* 2024, DOI :10.1007/s42967-024-00396-9.
- [50] J. Bolte, A. Daniilidis and A. Lewis, "The Łojasiewicz inequality for nonsmooth subanalytic functions with applications to subgradient dynamical systems," *SIAM J. Optim.* vol. 17, no. 4, pp. 1205–1223, 2006.
- [51] J. Bochnak, M. Coste and M. F. Roy, *Real Algebraic Geometry*, Ergebnisse der Mathematik und ihrer Grenzgebiete, Springer, Berlin, 1998.
- [52] H.-Y. Yan, Y.-M. Huang and Y. Yu, "A matrix rank minimization-based regularization method for image restoration," *Digit. Signal Process.* vol. 130, 103694, 2022.
- [53] H. Attouch, J. Bolte and B. F. Svaiter, "Convergence of descent methods for semi-algebraic and tame problems: proximal algorithms, forward-backward splitting, and regularized Gauss-Seidel methods," *Math. Program.* vol. 137, pp. 91–29, 2013.
- [54] H. Attouch, J. Bolte, P. Redont and A. Soubeyran, "Proximal alternating minimization and projection methods for nonconvex problems: an approach based on the Kurdyka-Łojasiewicz inequality," *Math. Oper. Res.* vol. 35, no. 2, pp. 438–457, 2010.
- [55] Z. Wang, A. C. Bovik, H. R. Sheikh and E. P. Simoncelli, "Image quality assessment: from error visibility to structural similarity," *IEEE Trans. Image Process.* vol. 13, no. 4, pp.600-612, 2004.
- [56] W. Dong, G. Shi and X. Li, "Nonlocal image restoration with bilateral variance estimation: a low-rank approach," *IEEE Trans. Image Process.* vol. 22, no. 2, pp. 700-711, 2013.